Variability in supermassive black-hole accretion rates in fuzzy dark matter cores due to black-hole wandering

Eric Ludwig,[1,2] Philip Mocz,[2] and Victor H. Robles[1]

[1]*Rensselaer Polytechnic Institute, Department of Physics, Applied Physics, and Astronomy, 110 8th Street, Troy, New York 12180, USA*

[2]*Center for Computational Astrophysics, Flatiron Institute, 162 5th Avenue, New York, New York 10010, USA*

(Received 6 February 2026; revised 28 May 2026; accepted 1 July 2026; published 26 August 2026)

Soliton cores in fuzzy dark matter (FDM) deepen nuclear potentials and have been proposed to strongly boost Bondi accretion, potentially aiding rapid black-hole growth at high redshift. We test this in *live* Schrödinger-Poisson FDM cores coupled to isothermal gas, evolving a moving black hole (BH) that grows via a strictly mass-conserving sink. We measure boosts relative to the initial mean-density Bondi rate. Low-mass seeds ($M_{\mathrm{BH,init}} \lesssim 10^6 M_\odot$) do not sustain large boosts: BH wandering and soliton sloshing drive bursty accretion with dense gas only intermittently present near the BH. Intermediate seeds ($M_{\mathrm{BH,init}} \sim 10^7 M_\odot$) produce the most durable enhancement, reaching $\mathcal{O}(10^2)$ boosts for sound speed $c_s = 60\ \mathrm{km\,s^{-1}}$, while hotter gas approaches near-background Bondi rates. High-mass seeds ($M_{\mathrm{BH,init}} \sim 10^8 M_\odot$) quickly exhaust the sink-scale reservoir and become supply limited, suppressing long-lived growth despite the deepened potential. In general, central-potential deepening (e.g., by a soliton halo) does not guarantee long-lived fueling: sustained boosts emerge only when the black hole remains dynamically confined within the dense nuclear gas region. Our results suggest the supermassive black-hole formation channels relying on soliton-enhanced accretion alone are unlikely to provide sufficient early growth.

DOI: 10.1103/rvfk-89yg

I. INTRODUCTION

The era of the James Webb Space Telescope (JWST) has rapidly expanded the census of accreting black holes at $z \gtrsim 10$ and luminous quasars with inferred dynamical masses $\gtrsim 10^9 M_\odot$ already in place by $z \sim 7$ [1–7]. Proposed pathways for producing the initial black-hole seeds span Pop III remnants [8,9], heavy seeds via direct collapse [10–12], and intermediate-mass seeds from runaway stellar mergers [13,14]. The challenge is not merely seed formation, but sustaining the *fueling history* needed to reach these masses on a short cosmic timeline: light-seed scenarios generally demand long duty cycles near (or above) the Eddington rate [15–19], while heavier seeds still require rapid growth that exceeds simple Bondi-type estimates [20,21]. Regardless of the seeding channel, assembling a $\gtrsim 10^9 M_\odot$ supermassive black hole (SMBH) at high redshift requires efficiently delivering gas to subkiloparsec scales in environments that are turbulent, time dependent, and strongly shaped by feedback [22–25]. Many models invoke dense, long-lived nuclear reservoirs and steady inflow; whether such reservoirs form and persist in early galaxies remains uncertain [24,25]. A recurring issue is that simple spherical accretion scalings [26] can underpredict the supply needed unless the central gas density remains extremely high and the BH-gas relative velocities remain low for extended periods.

Ultralight dark matter (ULDM) [27–33] scenarios offer a qualitatively different dark-sector framework. In these models the dark matter is a bosonic field with an extremely small mass, typically in the range $m \sim 10^{-22}$–10^{-6} eV and often realized as an axionlike particle. Such ultralight fields arise naturally in high-energy theory, for example in constructions related to the quantum chromodynamics axion [34] and in string theory compactifications [35], which can naturally yield a spectrum of light pseudoscalar (axionlike) degrees of freedom spanning many orders of magnitude in mass. Within this broader class, the mass range $m_{\mathrm{FDM}} \sim 10^{-22}$–$10^{-20}$ eV is commonly referred to as *fuzzy* dark matter (FDM) [36], where the associated de Broglie wavelength reaches astrophysical (kiloparsec) scales and the wave nature of the field becomes dynamically important on halo scales. Ultrafaint dwarf galaxies place important constraints on this parameter space, with some analyses favoring substantially heavier boson masses [37]. However, the interpretation of these constraints

Published by the American Physical Society under the terms of the Creative Commons Attribution 4.0 International license. Further distribution of this work must maintain attribution to the author(s) and the published article's title, journal citation, and DOI.

depends on the modeling of satellite stellar dynamics and in capturing nonlinear subhalo-host system evolution in self-consistent ULDM halos [38]. Recent simulations suggest that Segue 1-like systems can arise at $m = 10^{-22}$ eV as near-disruption remnants, with their observed surface-density and velocity-dispersion profiles broadly matched in selected models once the nonlinear interplay between ULDM-induced heating, internal stellar relaxation, and stripping of outer stars is accounted for [39]. Other dwarf-galaxy studies likewise have found agreement with FDM masses in the range considered here, depending on the modeling assumptions [40,41]. On these scales, the same wave dynamics that suppress the small-scale structure [32,42] also imply inherently time-dependent, nonparticle-like halo behavior [43–45], motivating treatments in which the central potential and local gas environment are not assumed to be static. For a recent overview of FDM phenomenology and Schrödinger-Poisson simulation methods, see [46,47].

In the fuzzy regime, Schrödinger-Poisson simulations show that halos develop dense central soliton cores embedded in an interference-dominated envelope [48]. These coherent, ground-statelike cores can deepen the central potential and raise nuclear gas densities relative to comparable cold-dark-matter halos. In idealized calculations, this has been argued to enhance Bondi-like accretion onto embedded BHs: [49] model a static soliton potential coupled to an effectively infinite, homogeneous gas reservoir and report large accretion "boost factors" relative to the standard Bondi rate at fixed ambient density and temperature. Here we test whether such enhancements survive in a more realistic, time-dependent setting with self-consistent BH growth, BH/soliton motion, and a finite gas reservoir—i.e., whether soliton-driven boosting is generically *sustained* or instead fragile once dynamics and supply are treated consistently.

We address this question with controlled numerical experiments. We evolve a coupled FDM-gas-BH system using the time-dependent Schrödinger-Poisson (SP) equations for the FDM field and isothermal hydrodynamics for the gas, allowing both the BH and the soliton to move self-consistently in the combined potential. We grow the BH with a strictly mass-conserving, fixed-radius sink prescription—gas removed within $r_{\rm sink}$ is added to the BH mass each time step—following the FLASH sink-particle methodology [50,51]. Since the sub-$r_{\rm sink}$ accretion flow is not resolved in our simulations, we use this standard sink-particle formalism as a robust subgrid closure that conserves mass by construction and cleanly isolates supply limitation within the resolved control volume. This enables a direct, time-resolved comparison between the analytic Bondi-Hoyle-Lyttleton "target" rate and the mass-conserving sink accretion rate.

Our aims are to (1) reinterpret soliton-induced boosted-Bondi expectations once BH-gas dynamics are treated consistently, and (2) identify simple control parameters that determine when soliton-deepened potentials materially assist BH growth. We find that relative motion of BH-soliton wandering and finite gas supply jointly regulate both the instantaneous analytic accretion demand and the mass-conserving sink accretion.

II. THEORY BACKGROUND

We evolve the self-gravitating Schrödinger-Poisson system for the FDM field ψ,

$$i\hbar\partial_t\psi(\mathbf{x},t) = -\frac{\hbar^2}{2m}\nabla^2\psi + m\Phi\psi, \tag{1}$$

with gravity sourced by FDM, gas, and a BH in a periodic domain with mean-subtracted densities

$$\begin{gathered}\nabla^2\Phi = 4\pi G[\rho_{\rm FDM} + \rho_{\rm gas} + \rho_{\rm BH} - \langle\rho_{\rm tot}\rangle],\\ \rho_{\rm FDM} \equiv |\psi|^2,\\ \rho_{\rm BH}(\mathbf{x},t) \equiv [\rho_{\rm BH,CIC}(\mathbf{x},t)\star G_{r_{\rm sink}}(\mathbf{x})],\\ \int \rho_{\rm BH} d^3x = M_{\rm BH}(t).\end{gathered} \tag{2}$$

Here $\rho_{\rm BH,CIC}$ is the cloud-in-cell (trilinear) deposition of the BH mass $M_{\rm BH}(t)$ onto the mesh at position $\mathbf{x}_{\rm BH}(t)$ (nonzero only on the eight neighboring cells, with weights summing to unity), and $G_{r_{\rm sink}}$ is a Gaussian sink-scale kernel of width $r_{\rm sink}$ applied via Fourier filtering, $\tilde\rho_{\rm BH}(\mathbf{k}) = \tilde\rho_{\rm BH,CIC}(\mathbf{k})\exp[-k^2 r_{\rm sink}^2/2]$. In our runs we take $r_{\rm sink} = 2.5\Delta x$, with Δx being the cell size, and $M_{\rm BH}(t) = M_{\rm seed}(t) + M_{\rm acc}(t)$, where the accreted mass, $M_{\rm acc}$, is determined by the gas mass removed from the sink each time step. Over the 0.5 Gyr window used to measure accretion, this corresponds to $\simeq 5.5\times10^4$ time steps, with a typical step $\Delta t_{\rm eff} \simeq 9.1\times10^{-6}$ Gyr.

The soliton core solutions are described by [48]

$$\rho_{\rm sol}(r) = \rho_0\left[1 + 0.091\left(\frac{r}{r_c}\right)^2\right]^{-8}, \tag{3}$$

where r_c is the core radius and ρ_0 is the central density given by

$$\rho_0 \simeq 3.1\times10^{15}\left(\frac{2.5\times10^{-22}\ \text{eV}}{m}\right)^2\left(\frac{\text{kpc}}{r_c}\right)^4\frac{M_\odot}{\text{Mpc}^3}. \tag{4}$$

Numerical simulations and analytic arguments relate the soliton to its host halo via approximate core-halo scalings, e.g. $r_c \propto m_{22}^{-1}M_h^{-1/3}$ and $M_{\rm sol} \propto m_{22}^{-1}M_h^{1/3}$ at fixed redshift, where $m_{22} \equiv m/10^{-22}$ eV [e.g. [49,52]]. For halo masses $M_h \sim 10^{10}$–$10^{11}M_\odot$ at $z \sim 7$–9 and $m \sim 10^{-22}$ eV, this implies central solitons of $M_{\rm sol} \sim 10^7$–$10^9 M_\odot$ and kiloparsec-scale cores, so the soliton can carry a significant

fraction of the inner mass budget and substantially deepen the central potential.

In fully relaxed FDM halos, the soliton does not remain perfectly fixed at the halo center. Interference with the surrounding turbulent envelope drives a stochastic center-of-mass "random walk" with an amplitude of order the core radius and characteristic timescales of order the core dynamical time [43]. Thus, even in the absence of any embedded BH, the central potential well is time dependent on dynamical timescales, and any BH embedded in the core can experience both soliton motion and internal structural oscillations [43,44] (Fig. 1).

Boost definitions: For gas with ambient density ρ_∞, sound speed c_s, and BH-gas relative velocity $v_{\rm rel}$, we adopt the classical Bondi-Hoyle-Lyttleton accretion rate [26,53,54]; for brevity, we refer to this expression as the "Bondi" rate throughout this work,

$$\dot{M}_{\rm target} = 4\pi\lambda \frac{(GM_{\rm BH})^2 \rho_\infty}{(c_s^2 + v_{\rm rel}^2)^{3/2}}. \tag{5}$$

Here G is Newton's gravitational constant, $M_{\rm BH}$ is the instantaneous BH mass, c_s is the (isothermal) sound speed of the gas, and $v_{\rm rel}$ is the BH-gas relative speed. The quantity ρ_∞ denotes the ambient gas density entering the Bondi estimate; in our simulations we estimate ρ_∞ from the resolved flow in a thin shell just outside the sink/control radius $r_{\rm sink}$. The parameter λ is a dimensionless factor of order unity that depends on the equation of state and the specific Bondi prescription. In what follows we refer to $\dot{M}_{\rm target}$ as the analytic target rate: it is the instantaneous Bondi rate that the local flow *demands*, based on the measured ambient density and relative velocity.

To factor out the global thermodynamics and the simulation box mean gas content, we compare all rates to a single, spatially homogeneous reference value evaluated at the initial box-mean gas density $\bar{\rho}_{\rm gas,0}$ and the chosen sound speed. We denote this as the background rate,

$$\dot{M}_{\rm bg}(\bar{\rho}_{\rm gas,0}, c_s; M_{\rm BH}) \equiv 4\pi\lambda \frac{(GM_{\rm BH})^2 \bar{\rho}_{\rm gas,0}}{c_s^3}, \tag{6}$$

which is just the Bondi rate for a BH of mass $M_{\rm BH}$ embedded in a uniform medium of density $\rho_{\rm gas}$ and sound speed c_s.

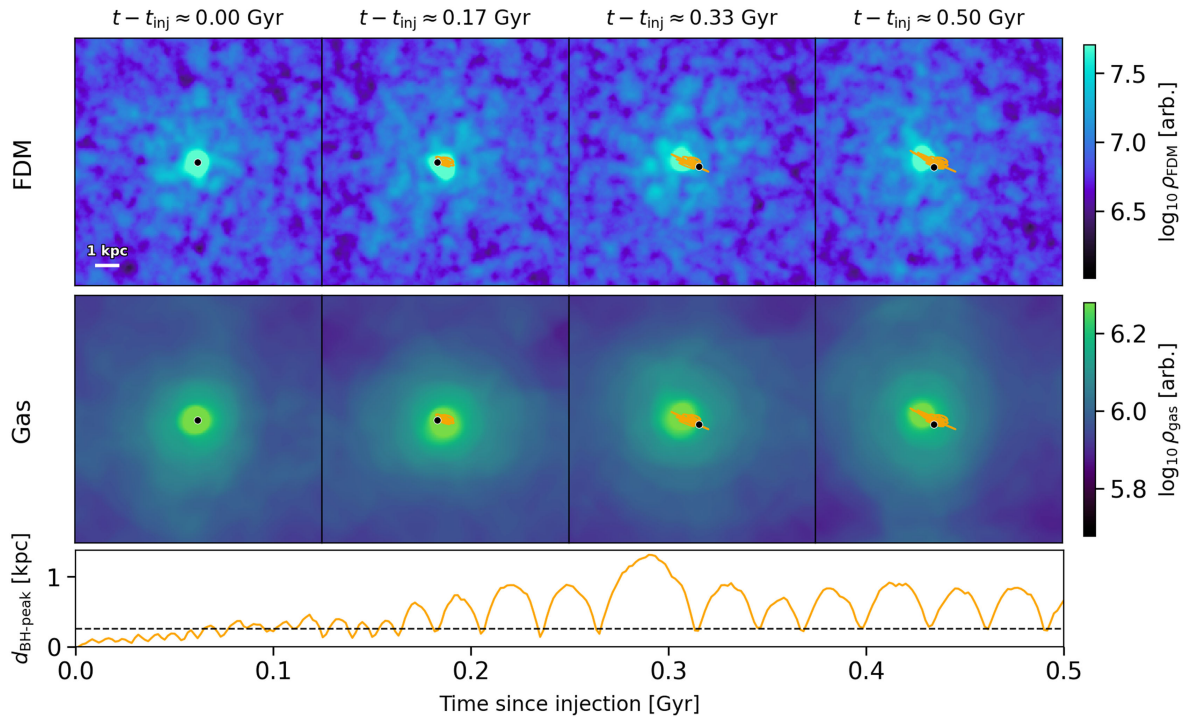


FIG. 1. Shown: $c_s = 70\ {\rm km\,s^{-1}}$ and $M_{\rm BH,init} = 10^6 M_\odot$ run; black-hole injection into a live soliton core and subsequent BH-core wandering under the time-dependent FDM + gas potential. Top: four midplane FDM density slices at times $t - t_{\rm inj} = \{0, 0.17, 0.33, 0.50\}$ Gyr; the marker indicates the BH position and the line traces the BH trajectory up to each snapshot. Middle: corresponding midplane gas density slices at the same times, shown with the same BH marker and trajectory overlay. Bottom: distance between the BH and the instantaneous soliton density peak, $d_{\rm BH\text{-}peak}$, as a function of time since injection (dashed line indicates the median core radius r_c). The BH mass grows via a strictly mass-conserving sink operating inside the fixed control radius $r_{\rm sink}$, while the soliton and gas respond self-consistently to the evolving potential.

Our primary boost quantity is the analytic boost,

$$\alpha_{\rm target} \equiv \frac{\dot{M}_{\rm target}}{\dot{M}_{\rm bg}(\bar{\rho}_{\rm gas,0}, c_s; M_{\rm BH})}, \tag{7}$$

which measures how strongly the local density and velocity field due to the soliton would enhance (or suppress) the accretion rate relative to the homogeneous background.

The simulations also provide the sink accretion rate $\dot{M}_{\rm sink}$, defined as the strictly mass-conserving rate obtained from the gas actually removed inside the sink/control volume at each step. We first summarize how well the flow keeps up with the analytic demand by defining

$$\kappa \equiv \frac{\dot{M}_{\rm sink}}{\dot{M}_{\rm target}}, \tag{8}$$

so that $\kappa \approx 1$ means that the flow supplies essentially the full analytic target rate, while $\kappa < 1$ indicates that the sink rate falls short (for example, because the gas inside the sink radius has been depleted and the flow has become explicitly supply limited).

Using $\alpha_{\rm target}$ and κ, it is convenient to define a corresponding sink boost,

$$\alpha_{\rm sink} \equiv \kappa \alpha_{\rm target} = \frac{\dot{M}_{\rm sink}}{\dot{M}_{\rm bg}(\bar{\rho}_{\rm gas,0}, c_s; M_{\rm BH})}, \tag{9}$$

which is the actual enhancement of the numerically realized flow above the same background rate. By construction, $\alpha_{\rm sink} \leq \alpha_{\rm target}$ whenever $\kappa \leq 1$.

To diagnose when the accretion becomes supply limited in our closed-box experiments, we track the total gas mass of the reservoir in the domain,

$$M_{\rm res}(t) \equiv \int_{V_{\rm box}} \rho_{\rm gas}(\mathbf{x}, t) d^3x, \tag{10}$$

and its normalized form $M_{\rm res}(t)/M_{\rm res}(t_0)$ (Fig. 3). In practice, sustained departures with $\kappa < 1$ occur only once the global reservoir has been strongly depleted; prior to that point, the sink rate typically remains demand limited with $\kappa \simeq 1$.

III. METHODS

Our simulations isolate the coupled FDM-BH-gas system in a periodic box while retaining the ingredients most relevant for boosted accretion. We perform them with a new JAX-based Schrödinger-Poisson + hydrodynamics code built on the JAXION framework [55]. In this work we extend JAXION by (i) adding a moving BH sink particle that contributes to the total gravitational potential, and (ii) evolving an isothermal gas component on the same mesh that is gravitationally coupled to the FDM and allowed to accrete conservatively onto the BH inside a fixed-radius control volume.

TABLE I. Simulation parameters and run grid. *Note:* The suite comprises six runs spanning the $(c_s, M_{\rm BH,init})$ grid. Here Δx denotes the grid cell width.

Parameter	Symbol	Value(s)
Boson mass	m_ψ	10^{-22} eV
Grid resolution	N	256^3
Box size	L	10 kpc
Mean total density	$\bar{\rho}_{\rm tot,0}$	$10^7 M_\odot$ kpc^{-3}
FDM fraction	$f_{\rm FDM}$	0.9
Gas fraction	$f_{\rm gas}$	0.1
Sound speed	c_s	$\{60, 70\}$ km s^{-1}
BH seed mass	$M_{\rm BH,init}$	$\{10^6, 10^7, 10^8\} M_\odot$
Sink radius	$r_{\rm sink}$	$2.5\Delta x$
Postinjection duration	$T_{\rm post}$	0.5 Gyr
Typical time step	$\Delta t_{\rm eff}$	9.1×10^{-6} Gyr
Time steps in $T_{\rm post}$	$N_{\rm step}$	5.5×10^4

We evolve a coupled FDM-gas-BH system in a periodic box; the numerical and physical parameters are summarized in Table I. The gas is evolved isothermally having an adiabatic index $\gamma = 1$ and sound speed $c_s \in \{60, 70\}$ km s^{-1} (corresponding to $T \simeq 2.6 \times 10^5$ K and 3.6×10^5 K). In our fiducial volume the initial conditions correspond to $M_{\rm FDM,box} \simeq 10^{10} M_\odot$ and a central soliton of total mass $M_{\rm sol} \simeq 2 \times 10^9 M_\odot$. Prior to BH injection, we generate the FDM halo by merging solitonic cores and evolving until it relaxes to a quasisteady soliton+interference (granular) state [43]. After injection, each run is evolved for $T_{\rm post} \simeq 0.5$ Gyr and all accretion diagnostics are measured over this postinjection interval.

This setup generalizes earlier static potential or fixed-BH-mass models (e.g., [56]) by allowing (i) genuine BH growth, (ii) BH and soliton motion (random walk, sloshing, migration), and (iii) explicit tracking of the finite local reservoir. It also parallels velocity-focused work [57,58] by tying the effective Bondi rate to c_s, $v_{\rm rel}$, and the evolving density field in a live core. These are closed-box experiments: we do not impose cosmological inflow, cooling-driven resupply, or external fueling. Thus, depletion reflects exhaustion of the resolved reservoir rather than feedback-driven evacuation.

The BH position is advanced using the local gravitational acceleration from the total SP + gas potential, allowing migration via dynamical friction and stochastic excursions driven by potential fluctuations. These modulate sampled density and the BH-gas relative velocity.

Ambient quantities for the analytic Bondi rate, Eq. (5), are taken from the resolved flow in a thin shell just outside $r_{\rm sink}$. When the BH is near the soliton/gas density peak this samples the highest-density gas accessible at the resolved scale; BH wandering shifts the shell off-peak, typically lowering ρ_∞ and increasing $v_{\rm rel}$, and thus modulates $\dot{M}_{\rm target}$. Mass removal occurs only inside $r_{\rm sink}$, is capped by the available mass each step, and the removed mass is added to

the BH, defining the sink-measured rate $\dot{M}_{\rm sink}$. This allows the analytic demand and the strictly mass-conserving rate to be compared at every snapshot.

At each snapshot, we evaluate the background Bondi rate $\dot{M}_{\rm bg}(\bar{\rho}_{\rm gas,0}, c_s; M_{\rm BH})$ from the initial box-mean gas density and chosen sound speed, compute $\dot{M}_{\rm target}$ from Eq. (5), and measure $\dot{M}_{\rm sink}$ from gas actually removed inside $r_{\rm sink}$. Equations (7)–(10) then give $\alpha_{\rm target}$, $\alpha_{\rm sink}$, κ, and $M_{\rm res}(t)/M_{\rm res}(t_0)$. We also record $M_{\rm BH}$, ρ_∞, $r_{\rm B}$, BH-soliton separation, and central densities; $M_{\rm res}(t)/M_{\rm res}(t_0)$ identifies when the system becomes globally fuel limited.

IV. RESULTS

For $M_{\rm BH} \lesssim 10^7 M_\odot$, accretion is demand limited and boost variability is set primarily by dynamics. The analytic boost $\alpha_{\rm target}$ fluctuates as the BH samples different ρ_∞ and $v_{\rm rel}$ along its trajectory and the sink boost $\alpha_{\rm sink}$ closely tracks $\alpha_{\rm target}$ with $\kappa \simeq 1$ whenever gas remains available inside $r_{\rm sink}$. Thus, variability in both boosts is dominated by BH motion and time-dependent soliton/gas structure rather than by supply limitation.

At fixed $M_{\rm BH}$, cooler gas runs ($c_s = 60$ km s^{-1}) attain systematically larger boosts than hotter gas, consistent with the Bondi scaling $\dot{M} \propto {c_s}^{-3}$. In the $M_{\rm BH} = 10^6 M_\odot$ cases, the BH can spend extended intervals outside the soliton core (often at $r \gtrsim r_c$), during which it samples lower densities and the boosts approach unity, $\alpha_{\rm target} \simeq \alpha_{\rm sink} \simeq 1$; elevated boosts occur in intermittent episodes when the BH returns to the dense central region. The $M_{\rm BH} = 10^7 M_\odot$ seeds remain more tightly confined to the central region than the $10^6 M_\odot$ seeds, and therefore sustain higher typical boosts and longer high-$\alpha_{\rm sink}$ episodes in both sound-speed setups.

For $M_{\rm BH} \sim 10^8 M_\odot$, the target (Bondi) rate can become very large when the BH sits in dense gas with small $v_{\rm rel}$, producing large instantaneous $\alpha_{\rm target}$ (and correspondingly large $\alpha_{\rm sink}$ while gas remains available inside the sink region). A persistent separation between analytic and sink boosts occurs only after the gas reservoir inside $r_{\rm sink}$ is drained: as $M_{\rm res}$ declines, the sink rate can no longer satisfy the analytic demand, yielding $\alpha_{\rm sink} < \alpha_{\rm target}$ and $\kappa < 1$ (Fig. 3). Before depletion, both $\alpha_{\rm target}$ and $\alpha_{\rm sink}$ vary together in response to the same dynamical changes in density and $v_{\rm rel}$. Overall, boosted phases are intermittent and track BH core sampling, except in the $M_{\rm BH} \sim 10^8 M_\odot$ runs where depletion drives sustained $\kappa < 1$.

V. DISCUSSION

Our experiments connect static-potential soliton "boost" estimates with effectively infinite reservoirs [49] to velocity-focused live-core dynamics [57,58]. In a live FDM core, the enhancement is not set by the potential depth alone: thermodynamics and dynamics jointly determine the instantaneous Bondi demand and whether the resolved flow can continuously supply it.

At fixed $M_{\rm BH}$, lowering c_s increases the analytic demand ($\dot{M} \propto c_s^{-3}$) and also alters the core state sampled by the BH. The lower-c_s runs develop more centrally concentrated FDM + gas cores (Fig. 2) and smoother boost

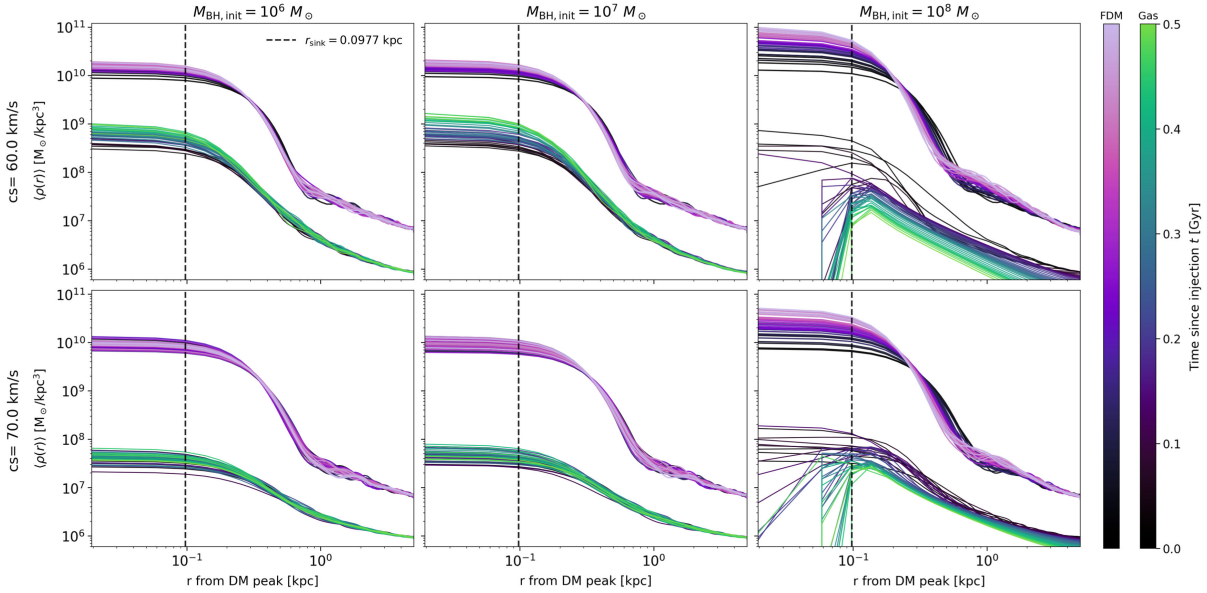


FIG. 2. Radial density profiles of the FDM and gas measured about the instantaneous FDM density peak, illustrating thermodynamic contraction and BH-driven core evolution. Columns show the three BH seed masses ($M_{\rm BH,init} = 10^6, 10^7, 10^8 M_\odot$); rows show the two sound speeds ($c_s = 60$ and 70 km s^{-1}). Within each panel, profiles are plotted at multiple times spanning the postinsertion evolution; the curve color encodes the simulation time (Gyr) as indicated by the accompanying colorbar. Lower-c_s runs develop a more centrally concentrated gas + FDM configuration, while higher-mass seeds more strongly restructure the inner gas profile as accretion proceeds.

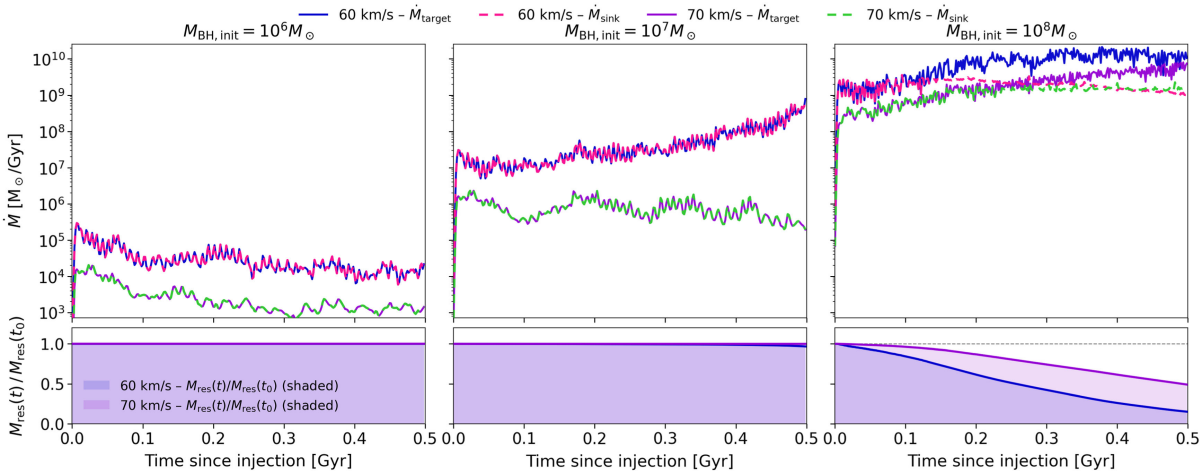


FIG. 3. Black hole accretion histories and global gas reservoir for the six fiducial runs. Each column corresponds to a different initial BH mass ($M_{\rm BH,init} = 10^6, 10^7, 10^8 M_\odot$). Top: analytic accretion rate $\dot{M}_{\rm target}$ (solid) and mass-conserving sink rate $\dot{M}_{\rm sink}$ (dotted) versus time since injection, with both sound-speed runs ($c_s \approx 60$ and 70 km s^{-1}) overplotted in each panel. Bottom: corresponding evolution of the total gas mass in the box, normalized to its value at injection, $M_{\rm res}(t)/M_{\rm res}(t_{\rm inj})$, again with both sound speeds overplotted; the shaded region indicates depletion relative to the initial reservoir. Low-mass seeds remain close to the target rate for most of the evolution, while the most massive BHs rapidly become globally fuel limited as the box reservoir is drained and $\dot{M}_{\rm sink} \ll \dot{M}_{\rm target}$.

histories (Fig. 4), consistent with faster relaxation toward a quasisteady central configuration. In particular for $c_s \sim 70$ km s^{-1}, the $M_{\rm BH} = 10^6 M_\odot$ seed is more orbit-dominated and spends long intervals outside the dense core, so $\alpha_{\rm target}$ and $\alpha_{\rm sink}$ often collapse toward unity.

Our parameter choice is also limited by numerical fidelity: we restrict to $c_s \in \{60, 70\}$ km s^{-1} because, in an isothermal setup at fixed resolution, reducing c_s shrinks the Jeans length $\lambda_J \propto c_s \rho^{-1/2}$ and would violate the Truelove criterion [59], driving artificial runaway central collapse. Across this range, the BH-gas relative speed is typically $v_{\rm rel} \sim 40$–150 km s^{-1} for $M_{\rm BH,init} = 10^6 M_\odot$, $\sim$40–80 km s^{-1} for $10^7 M_\odot$, and $\sim$25–60 km s^{-1} for $10^8 M_\odot$, with only weak dependence on c_s. Because $\dot{M}_{\rm target} \propto \rho_\infty (c_s^2 + v_{\rm rel}^2)^{-3/2}$, the $10^6 M_\odot$ runs often satisfy $v_{\rm rel} \gtrsim c_s$, so further decreases in c_s would yield only modest changes (diminishing returns once $c_s \ll v_{\rm rel}$) and would mainly amplify brief near-core episodes rather than the long off-center intervals. For 10^7–$10^8 M_\odot$ seeds, $v_{\rm rel}$ is typically smaller and c_s is comparable to or larger than $v_{\rm rel}$, so lowering c_s can substantially increase the demand, both directly and indirectly via stronger central contraction and enhanced BH confinement; in our closed-box setup, that larger demand also tends to hasten the onset of explicit supply limitation once gas within $r_{\rm sink}$ is depleted. Thus the $10^6 M_\odot$ runs remain dynamics dominated: lower c_s would mostly boost only brief near-core phases (e.g., the initial peak), not the long orbit-dominated intervals off center.

At fixed thermodynamics, varying $M_{\rm BH}$ controls both core sampling and depletion: increasing $M_{\rm BH}$ strengthens dynamical friction and central confinement, but it also raises demand and can accelerate draining of the local reservoir. This yields an intermediate regime at $M_{\rm BH} = 10^7 M_\odot$, which remains more tightly core bound than $10^6 M_\odot$ but does not rapidly drain gas inside $r_{\rm sink}$ like $10^8 M_\odot$; the effect is strongest for $c_s = 60$ km s^{-1}, where core contraction enhances confinement and produces the longest high-α duty cycles among the nonsupply-limited runs (Fig. 4).

Finally, comparing sink accretion to analytic demand isolates when boosting is realized. While sufficient gas remains inside $r_{\rm sink}$, $\alpha_{\rm sink}$ closely tracks $\alpha_{\rm target}$ with $\kappa \approx 1$; sustained $\kappa < 1$ is tied to depletion of the sink control volume, not an imposed ceiling on the prescription. In cosmological settings with sustained inflow from larger scales, the sink control volume could be continually refueled, so depletion-driven $\kappa < 1$ may be less relevant and $\dot{M}_{\rm sink}$ would track the local demand until limited by galaxy-scale supply/feedback. Moreover, our $10^8 M_\odot$ seed in a fixed-mass core is intentionally idealized; establishing how such a massive BH would arise in this environment requires separate modeling. Overall, while soliton-deepened potentials can support large instantaneous accretion demand in static-reservoir estimates, in live FDM cores the sink boosts and their duty cycle are set by orbital sampling, soliton sloshing, and, in our closed-box simulation, finite supply (Fig. 5).

Our simulations are isolated and omit several astrophysical ingredients that could shift the quantitative confinement and supply thresholds. Cosmological inflow or cooling-driven resupply could maintain the nuclear reservoir and keep $\dot{M}_{\rm sink}$ closer to $\dot{M}_{\rm target}$ for longer, while feedback, turbulence, angular momentum support, and galaxy-scale supply limits could instead shorten the lifetime of dense gas near the BH. Stars, nuclear star clusters,

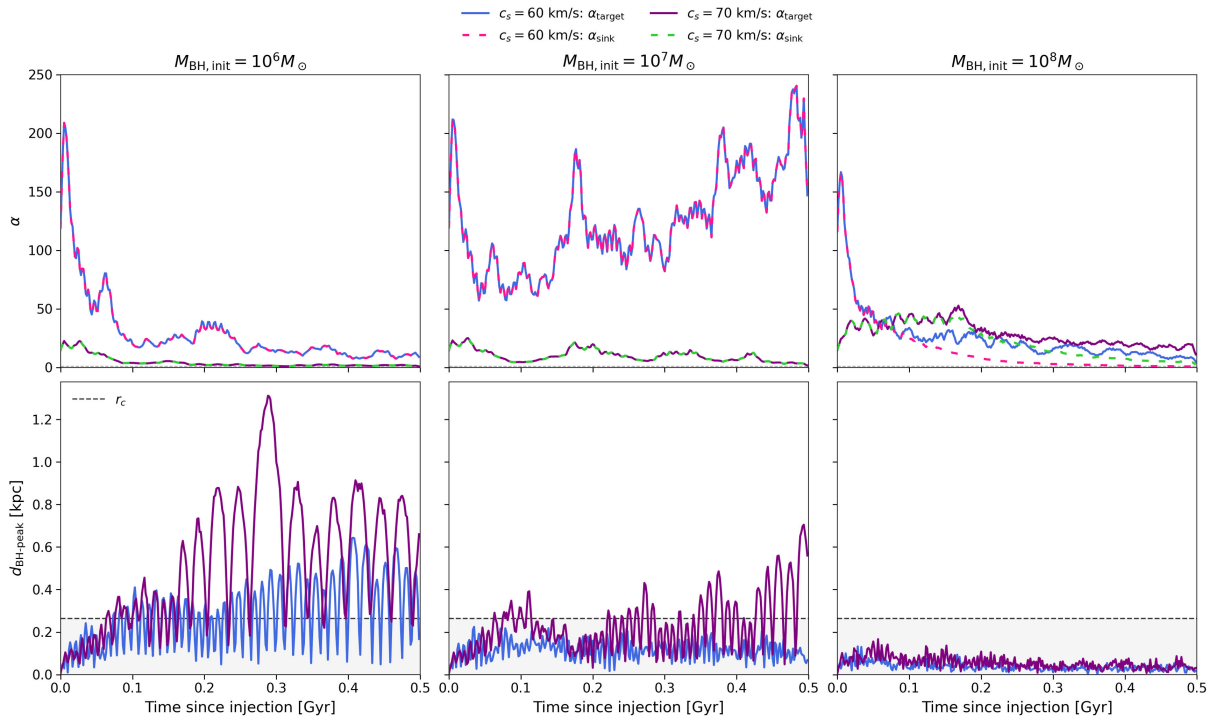


FIG. 4. Boost evolution and BH-core separation for the same six fiducial runs and 2×3 layout as Fig. 3, with both sound-speed cases ($c_s \approx 60$ and 70 km s^{-1}) overplotted in each panel. In each top panel, we show the analytic boost factor $\alpha_{\rm target}$ [solid; Eq. (7)] and the sink boost $\alpha_{\rm sink}$ [dotted; Eq. (9)] versus time since injection. In each bottom panel, we show the BH distance from the instantaneous soliton density peak, $d_{\rm BH\text{-}peak}$; the horizontal dashed line marks the median soliton core radius r_c. Elevated boosts occur preferentially during intervals when the BH remains within (or repeatedly revisits) the soliton core, while sustained divergences between $\alpha_{\rm sink}$ and $\alpha_{\rm target}$ arise once local and/or global gas depletion sets in for the highest-mass runs.

or additional compact objects could also enhance the effective dynamical friction acting on the BH. Previous high-resolution studies of massive black-hole seed dynamics have shown that BHs embedded in surrounding stellar systems or nuclear star clusters can sink more efficiently toward the galactic center, whereas stripped BHs may stall at larger radii [60–66]. In our context, including such stellar components could keep the BH more tightly confined to the soliton/gas center and thereby increase the high-boost duty cycle. However, modeling

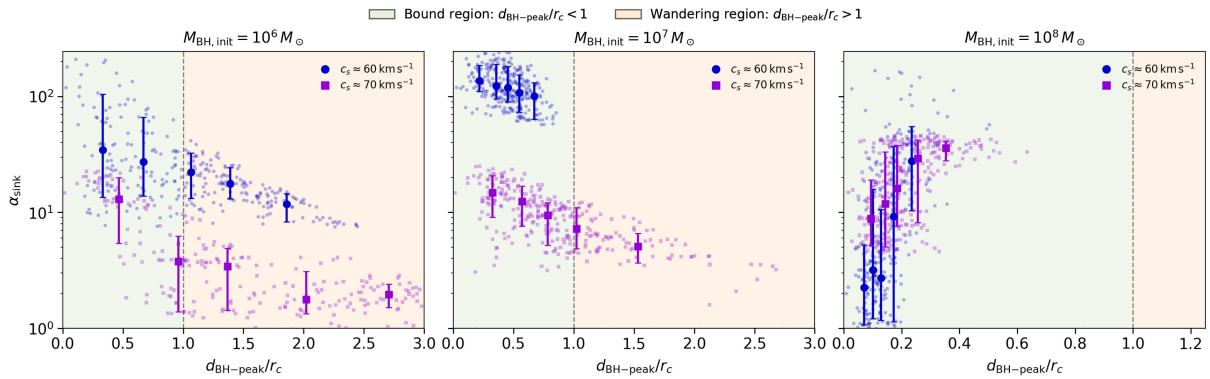


FIG. 5. Sink boost as a function of BH offset from the soliton core. Each panel corresponds to a BH seed mass ($M_{\rm BH,init} = 10^6, 10^7, 10^8 M_\odot$). The x axis shows the instantaneous BH-peak separation normalized by the soliton core radius, $d_{\rm BH\text{-}peak}/r_c$, and the y axis shows the sink boost $\alpha_{\rm sink}$ (log scale). Small points show individual simulation snapshots; large markers show binned medians with error bars indicating the scatter within each bin (as defined in the text/legend). Shaded regions separate a "core-bound" regime ($d_{\rm BH\text{-}peak}/r_c < 1$) from a "wandering" regime (> 1; vertical dashed line). Across the suite, boosts are highest when the BH remains core bound, and decline as the BH samples lower-density gas at larger offsets; the highest-mass case is additionally shaped by depletion-driven supply limitation.

this self-consistently requires resolving the coupled gas, stellar, BH, and dark-matter dynamics in a cosmological environment, so both this setup and ours should ultimately be revisited with dedicated cosmological simulations. Such effects could allow lower-mass seeds to behave more like the confined cases studied here, but would not by itself guarantee SMBH assembly: the confined cases show that maintaining the boost is only one requirement, while the total mass gained by high redshift still depends on the gas thermodynamics and on how efficiently inflow maintains dense, low-relative-velocity gas around the BH.

VI. CONCLUSIONS

In live, self-gravitating FDM soliton cores with conservative, fixed-radius sinks, accretion is regulated primarily by dynamics and becomes explicitly supply limited only after depletion in the most demanding cases. For $M_{\rm BH} \lesssim 10^7 M_\odot$, boosts are intermittent because BH motion controls how often the BH samples dense nuclear gas; in the hotter $c_s = 70\ {\rm km\,s^{-1}}$ case, the $10^6 M_\odot$ seed spends extended intervals outside the core, so boosts frequently approach unity. In this low-mass regime, any accretion-powered emission could therefore appear measurably off nuclear, an observational consequence we leave to future work (e.g., [67]). Sustained boosting is maximized for intermediate seeds ($M_{\rm BH} \sim 10^7 M_\odot$) in the cooler $c_s = 60\ {\rm km\,s^{-1}}$ runs, where confinement is strong without rapid local depletion. This behavior is not simply a consequence of the BH and soliton masses being comparable: for $M_{\rm sol} \simeq 2 \times 10^9 M_\odot$ we have $M_{\rm BH}/M_{\rm sol} \in \{5 \times 10^{-4}, 5 \times 10^{-3}, 5 \times 10^{-2}\}$ for $M_{\rm BH} \in \{10^6, 10^7, 10^8\} M_\odot$. When supply limitation occurs, it is depletion driven: only the $M_{\rm BH} \sim 10^8 M_\odot$ runs sustain $\kappa < 1$ after gas inside $r_{\rm sink}$ is exhausted. Overall, deep soliton potentials can raise instantaneous demand, but large, long-lived boosts are not generic in live cores.

A key implication when combined with the soliton picture of [48,52] is that FDM can plausibly provide the *potential* needed for large instantaneous Bondi demand in high-z halos, but soliton-enhanced accretion alone is unlikely to provide sufficient early SMBH growth: if the initial seed is too light to remain core bound, wandering suppresses the duty cycle of high-density sampling and the boost collapses toward unity. In that case, the central question shifts to how the BH reaches the confinement-favorable mass scale (e.g., via heavy seeding or an early growth phase not captured by a closed-box setup), after which soliton deepening can help sustain high demand only if nuclear gas is continuously replenished.

A. Implications for cored dark-matter halos

Large Bondi-like boosts require more than a deep central potential. The BH must remain colocated with the densest nuclear gas, and that gas must persist long enough to supply the implied demand. Our live FDM experiments provide a concrete example: even with a deep central potential, boosts become intermittent when the BH spends extended intervals outside the core, as wandering lowers the surrounding gas density near the BH and raises $v_{\rm rel}$, and becomes explicitly supply limited only after the gas inside $r_{\rm sink}$ is depleted.

The colocation requirement can arise in models where the central mass distribution is shallow or cored. In such systems, the restoring force and the phase-space structure that controls dynamical friction can differ substantially from a cuspy halo, allowing the inspiral to slow or stall before the BH remains embedded in the nuclear gas. Constant-density cores are well known to exhibit weakened or stalled dynamical friction in collisionless systems [68–71]. FDM is a particularly strong realization of this issue because its soliton combines a flat inner density profile with intrinsic time dependence from wave interference, random walk, and granular fluctuations, which can further perturb BH orbits [32,43,44,48,72].

Self-interacting dark matter (SIDM) provides an important cored-halo comparison because SIDM halos can form extended low-density cores, and simulations have found more off-center SMBHs and delayed SMBH growth in such systems [73,74]. At the same time, SIDM is not a one-to-one analog of FDM: self-interactions can modify the core phase-space structure, reduce or eliminate core stalling in some regimes, and drive core contraction or gravothermal evolution [75–77]. Thus the quantitative wandering amplitudes and boost duty cycles measured here should not be applied unchanged to SIDM, but the central requirement remains relevant: any boosted-accretion scenario in a cored halo must show both a mechanism that concentrates gas and a mechanism that keeps the BH colocated with that gas for a sufficiently long duty cycle.

This work made use of the following software packages: JAX [78], NumPy [79], Python [80], SciPy [81], Matplotlib [82], H5PY [83]. Software citation information aggregated using `The Software Citation Station` [84,85].

ACKNOWLEDGMENTS

E. L. acknowledges support from the Center for Computational Astrophysics Predoctoral Program and the NASA New York Space Grant Fellowship. Simulations were performed on the Flatiron Institute Rusty computing cluster. The Flatiron Institute is supported by the Simons Foundation.

DATA AVAILABILITY

The code used in this work is available at [86]. Simulation outputs and derived data products are available from the corresponding author upon reasonable request.

[1] E. Bañados, B. P. Venemans, C. Mazzucchelli, E. P. Farina, F. Walter, F. Wang, R. Decarli, D. Stern, X. Fan, F. B. Davies, J. F. Hennawi, R. A. Simcoe, M. L. Turner, H.-W. Rix, J. Yang, D. D. Kelson, G. C. Rudie, and J. M. Winters, Nature (London) **553**, 473 (2018).

[2] J. Yang, F. Wang, X. Fan, J. F. Hennawi, F. B. Davies, M. Yue, E. Banados, X.-B. Wu, B. Venemans, A. J. Barth, F. Bian, K. Boutsia, R. Decarli, E. P. Farina, R. Green, L. Jiang, J.-T. Li, C. Mazzucchelli, and F. Walter, Astrophys. J. Lett. **897**, L14 (2020).

[3] R. L. Larson *et al.* (Ceers Team), Astrophys. J. Lett. **953**, L29 (2023).

[4] V. Kokorev *et al.*, Astrophys. J. Lett. **957**, L7 (2023).

[5] Á. Bogdán, A. D. Goulding, P. Natarajan, O. E. Kovács, G. R. Tremblay, U. Chadayammuri, M. Volonteri, R. P. Kraft, W. R. Forman, C. Jones, E. Churazov, and I. Zhuravleva, Nat. Astron. **8**, 126 (2024).

[6] O. E. Kovács, Á. Bogdán, P. Natarajan, N. Werner, M. Azadi, M. Volonteri, G. R. Tremblay, U. Chadayammuri, W. R. Forman, C. Jones, and R. P. Kraft, Astrophys. J. Lett. **965**, L21 (2024).

[7] T. J. Looser *et al.*, Nature (London) **629**, 53 (2024).

[8] V. Bromm, Rep. Prog. Phys. **76**, 112901 (2013).

[9] K. Sugimura, T. Matsumoto, T. Hosokawa, S. Hirano, and K. Omukai, Astrophys. J. Lett. **892**, L14 (2020).

[10] J. H. Wise, J. A. Regan, B. W. O'Shea, M. L. Norman, T. P. Downes, and H. Xu, Nature (London) **566**, 85 (2019).

[11] F. Sassano, R. Schneider, R. Valiante, K. Inayoshi, S. Chon, K. Omukai, L. Mayer, and P. R. Capelo, Mon. Not. R. Astron. Soc. **506**, 613 (2021).

[12] L. Mayer, P. R. Capelo, L. Zwick, and T. Di Matteo, Astrophys. J. **961**, 76 (2024).

[13] K. Omukai, R. Schneider, and Z. Haiman, Astrophys. J. **686**, 801 (2008).

[14] B. Devecchi and M. Volonteri, Astrophys. J. **694**, 302 (2009).

[15] M. Smole, M. Micic, and N. Martinović, Mon. Not. R. Astron. Soc. **451**, 1964 (2015).

[16] K. Inayoshi, Z. Haiman, and J. P. Ostriker, Mon. Not. R. Astron. Soc. **459**, 3738 (2016).

[17] E. Pezzulli, M. Volonteri, R. Schneider, and R. Valiante, Mon. Not. R. Astron. Soc. **471**, 589 (2017).

[18] L. Mayer, Super-Eddington accretion; flow regimes and conditions in high-z galaxies, in *Formation of the First Black Holes*, edited by M. Latif and D. Schleicher (World Scientific, Singapore, 2019), pp. 195–222.

[19] K. Inayoshi, Astron. Herald **115**, 747 (2022).

[20] J. Jeon, B. Liu, V. Bromm, and S. L. Finkelstein, Mon. Not. R. Astron. Soc. **524**, 176 (2023).

[21] J. Jeon, V. Bromm, B. Liu, and S. L. Finkelstein, Astrophys. J. **979**, 127 (2025).

[22] T. Di Matteo, V. Springel, and L. Hernquist, Nature (London) **433**, 604 (2005).

[23] P. F. Hopkins and E. Quataert, Mon. Not. R. Astron. Soc. **407**, 1529 (2010).

[24] Y. Dubois, M. Volonteri, J. Silk, J. Devriendt, A. Slyz, and R. Teyssier, Mon. Not. R. Astron. Soc. **452**, 1502 (2015).

[25] D. Anglés-Alcázar, C.-A. Faucher-Giguère, E. Quataert, P. F. Hopkins, R. Feldmann, P. Torrey, A. Wetzel, and D. Kereš, Mon. Not. R. Astron. Soc. **472**, L109 (2017).

[26] H. Bondi, Mon. Not. R. Astron. Soc. **112**, 195 (1952).

[27] F. S. Guzmán, T. Matos, and H. B. Villegas, Astron. Nachr. **320**, 97 (1999).

[28] P. J. E. Peebles, Astrophys. J. Lett. **534**, L127 (2000).

[29] T. Matos, F. S. Guzmán, and L. A. Ureña-López, Classical Quantum Gravity **17**, 1707 (2000).

[30] C. G. Böhmer and T. Harko, J. Cosmol. Astropart. Phys. 06 (2007) 025.

[31] P. Sikivie and Q. Yang, Phys. Rev. Lett. **103**, 111301 (2009).

[32] L. Hui, J. P. Ostriker, S. Tremaine, and E. Witten, Phys. Rev. D **95**, 043541 (2017).

[33] L. Hui, Annu. Rev. Astron. Astrophys. **59**, 247 (2021).

[34] F. Wilczek, Phys. Rev. Lett. **40**, 279 (1978).

[35] A. Arvanitaki, S. Dimopoulos, S. Dubovsky, N. Kaloper, and J. March-Russell, Phys. Rev. D **81**, 123530 (2010).

[36] W. Hu, R. Barkana, and A. Gruzinov, Phys. Rev. Lett. **85**, 1158 (2000).

[37] N. Dalal and A. Kravtsov, Phys. Rev. D **106**, 063517 (2022).

[38] H. Y. J. Chan, H.-Y. Schive, V. H. Robles, A. Kunkel, G.-M. Su, and P.-Y. Liao, Mon. Not. R. Astron. Soc. **540**, 2653 (2025).

[39] Y.-M. Yang, X.-J. Bi, L. Wang, and P.-F. Yin, arXiv:2601.09403.

[40] S.-R. Chen, H.-Y. Schive, and T. Chiueh, Mon. Not. R. Astron. Soc. **468**, 1338 (2017).

[41] D. Wardana, K. Hayashi, M. Chiba, and E. G. M. Ferreira, arXiv:2603.07175.

[42] D. J. E. Marsh, Phys. Rep. **643**, 1 (2016).

[43] P. Mocz, M. Vogelsberger, V. H. Robles, J. Zavala, M. Boylan-Kolchin, A. Fialkov, and L. Hernquist, Mon. Not. R. Astron. Soc. **471**, 4559 (2017).

[44] D. Dutta Chowdhury, F. C. van den Bosch, V. H. Robles, P. van Dokkum, H.-Y. Schive, T. Chiueh, and T. Broadhurst, Astrophys. J. **916**, 27 (2021).

[45] D. Dutta Chowdhury, F. C. van den Bosch, P. van Dokkum, V. H. Robles, H.-Y. Schive, and T. Chiueh, Astrophys. J. **949**, 68 (2023).

[46] E. G. M. Ferreira, Astron. Astrophys. Rev. **29**, 7 (2021).

[47] H.-Y. Schive, Liv. Rev. Comput. Astrophys. **12**, 1 (2026).

[48] H.-Y. Schive, T. Chiueh, and T. Broadhurst, Nat. Phys. **10**, 496 (2014).

[49] H.-H. S. Chiu, H.-Y. Schive, H.-Y. K. Yang, H. Huang, and M. Gaspari, Phys. Rev. Lett. **134**, 051402 (2025).

[50] C. Federrath, R. Banerjee, P. C. Clark, and R. S. Klessen, Astrophys. J. **713**, 269 (2010).

[51] FLASH Center for Computational Science, FLASH User's Guide (version 4.8): Sink particles (section 21.4). https://flash.rochester.edu/site/flashcode/user_support/flash_ug_devel/node139.html (2024), last updated May 6, 2024; accessed 2025-12-02.

[52] H.-Y. Schive, M.-H. Liao, T.-P. Woo, S.-K. Wong, T. Chiueh, T. Broadhurst, and W.-Y. P. Hwang, Phys. Rev. Lett. **113**, 261302 (2014).

[53] F. Hoyle and R. A. Lyttleton, Proc. Cambridge Philos. Soc. **35**, 405. (1939).

[54] H. Bondi and F. Hoyle, Mon. Not. R. Astron. Soc. **104**, 273 (1944).

[55] P. Mocz, Jaxion, version 0.0.11, Zenodo (2026), https://github.com/JaxionProject/jaxion.

[56] C. Palomares-Chávez, I. Álvarez-Rios, and F. S. Guzmán, Phys. Rev. D **112**, 023545 (2025).
[57] L. Lancaster, C. Giovanetti, P. Mocz, Y. Kahn, M. Lisanti, and D. N. Spergel, J. Cosmol. Astropart. Phys. 01 (2020) 001.
[58] R. Boey, Y. Wang, E. Kendall, and R. Easther, Phys. Rev. D **109**, 103526 (2024).
[59] J. K. Truelove, R. I. Klein, C. F. McKee, J. H. Holliman, II, L. H. Howell, and J. A. Greenough, Astrophys. J. Lett. **489**, L179 (1997).
[60] M. Tremmel, F. Governato, M. Volonteri, A. Pontzen, and T. R. Quinn, Astrophys. J. Lett. **857**, L22 (2018).
[61] J. Bellovary, A. Hayoune, D. Chafla, R. J. Vincent, A. M. Brooks, C. R. Christensen, F. Munshi, M. Tremmel, T. Quinn, D. van Nest, J. Sligh, and S. Luzuriaga, Mon. Not. R. Astron. Soc. **505**, 5129 (2021).
[62] L. Ma, P. F. Hopkins, X. Ma, D. Anglés-Alcázar, C.-A. Faucher-Giguère, and L. Z. Kelley, Mon. Not. R. Astron. Soc. **508**, 1973 (2021).
[63] G. Ogiya, O. Hahn, C. M. F. Mingarelli, and M. Volonteri, Mon. Not. R. Astron. Soc. **493**, 3676 (2020).
[64] D. Mukherjee, Q. Zhu, G. Ogiya, C. L. Rodriguez, and H. Trac, Mon. Not. R. Astron. Soc. **518**, 4801 (2023).
[65] Y. Zhou, D. Mukherjee, N. Chen, T. Di Matteo, P. H. Johansson, A. Rantala, C. Partmann, U. N. Di Carlo, S. Bird, and Y. Ni, Astrophys. J. **980**, 79 (2025).
[66] D. Mukherjee, Y. Zhou, N. Chen, U. N. Di Carlo, and T. Di Matteo, Astrophys. J. **981**, 203 (2025).
[67] P. van Dokkum, I. Pasha, M. L. Buzzo, S. LaMassa, Z. Shen, M. A. Keim, R. Abraham, C. Conroy, S. Danieli, K. Mitra, D. Nagai, P. Natarajan, A. J. Romanowsky, G. Tremblay, C. M. Urry, and F. C. van den Bosch, Astrophys. J. Lett. **946**, L50 (2023).
[68] J. I. Read, T. Goerdt, B. Moore, A. P. Pontzen, J. Stadel, and G. Lake, Mon. Not. R. Astron. Soc. **373**, 1451 (2006).
[69] T. Goerdt, B. Moore, J. I. Read, J. Stadel, and M. Zemp, Mon. Not. R. Astron. Soc. **368**, 1073 (2006).
[70] J. A. Petts, A. Gualandris, and J. I. Read, Mon. Not. R. Astron. Soc. **454**, 3778 (2015).
[71] J. A. Petts, J. I. Read, and A. Gualandris, Mon. Not. R. Astron. Soc. **463**, 858 (2016).
[72] B. Bar-Or, J.-B. Fouvry, and S. Tremaine, Astrophys. J. **871**, 28 (2019).
[73] A. Di Cintio, M. Tremmel, F. Governato, A. Pontzen, J. Zavala, A. Bastidas Fry, A. Brooks, and M. Vogelsberger, Mon. Not. R. Astron. Soc. **469**, 2845 (2017).
[74] A. Cruz, A. Pontzen, M. Volonteri, T. R. Quinn, M. Tremmel, A. M. Brooks, N. N. Sanchez, F. Munshi, and A. Di Cintio, Mon. Not. R. Astron. Soc. **500**, 2177 (2021).
[75] S. Tulin and H.-B. Yu, Phys. Rep. **730**, 1 (2018).
[76] F. C. van den Bosch and S. Dattathri, Open J. Astrophys. **9**, 157701 (2026).
[77] F. Jiang, Z. Jiang, H. Zheng, L. C. Ho, K. Inayoshi, X. Shen, M. Vogelsberger, and W.-X. Feng, Astrophys. J. Lett. **996**, L19 (2026).
[78] J. Bradbury, R. Frostig, P. Hawkins, M. J. Johnson, C. Leary, D. Maclaurin, G. Necula, A. Paszke, J. VanderPlas, S. Wanderman-Milne, and Q. Zhang, JAX: Composable transformations of Python+NumPy programs (2018).
[79] C. R. Harris *et al.*, Nature (London) **585**, 357 (2020).
[80] G. Van Rossum and F. L. Drake, *Python 3 Reference Manual* (CreateSpace, Scotts Valley, CA, 2009).
[81] P. Virtanen *et al.* (SciPy 1.0 Contributors), Nat. Methods **17**, 261 (2020).
[82] J. D. Hunter, Comput. Sci. Eng. **9**, 90 (2007).
[83] A. Collette, *Python and HDF5* (O'Reilly, Sebastopol, CA, 2013).
[84] T. Wagg and F. S. Broekgaarden, arXiv:2406.04405.
[85] T. Wagg, F. Broekgaarden, P. Van-Lane, K. Wu, and K. Gültekin, Tomwagg/software-citation-station: v1.4 (2025).
[86] P. Mocz and E. Ludwig, quantum-jax, GitHub repository (2025), Github: github.com/pmocz/quantum-jax.